A STUDY OF THE EQUATORIAL IONIZATION ANOMALY FROM CHAMP SATELLITE ION DENSITY DATA

By

Tamirat Bekele

A THESIS SUBMITTED IN PARTIAL FULFILLMENT OF THE
REQUIREMENTS FOR THE DEGREE OF
MASTER OF SCIENCE IN PHYSICS
AT
ADDIS ABABA UNIVERSITY
ADDIS ABABA, ETHIOPIA
SEPTEMBER 2008

ADDIS ABABA UNIVERSITY
DEPARTMENT OF
PHYSICS

The undersigned hereby certify that they have read and recommend to the Faculty of Graduate Studies for acceptance a thesis entitled "**A study of the Equatorial Ionization Anomaly from CHAMP Satellite Ion Density Data**" by **Tamirat Bekele** in partial fulfillment of the requirements for the degree of **Master of Science in Physics**.

Dated: September 2008

Supervisor: _____
Dr. Esayas Belay

Readers: _____
Dr. Gizaw Mengistu

_____
Dr. Mulugeta Bekele

ADDIS ABABA UNIVERSITY

Date: **September 2008**

Author: **Tamirat Bekele**

Title: **A study of the Equatorial Ionization Anomaly from CHAMP Satellite Ion Density Data**

Department: **Physics**

Degree: **M.Sc.** Convocation: **August** Year: **2008**

Signature of Author

Table of Contents

List of Figures

Abstract

The equatorial ionization anomaly and equatorial electrojet are typical plasma dynamic processes of the equatorial ionosphere. Equatorial ionization anomaly is characterized as the occurrence of a trough in the ionization concentration at the equator and crests from about $\pm 15^0$ to $\pm 20^0$ in magnetic latitude in each hemisphere. Equatorial electrojet, on the other hand, is an intense electric current flowing in the E region of the ionosphere during the day time to the east direction.

The aim of this thesis is to study the seasonal, longitudinal, latitudinal and early evening characteristics of the equatorial ionization anomaly. In addition, we have drawn a tentative relationship between the equatorial ionization anomaly and equatorial electrojet. To accomplish these purposes, we have analyzed seven years (2000-2006) of CHAMP Satellite's ion density and magnetometer (current profiles) data. The results obtained show that the equatorial ionization anomaly varies rapidly with latitude as well as with longitude. It also exhibits a day to day and seasonal variation. The early evening anomaly structures are quite different from the noon times. In addition, both equatorial ionization anomaly and equatorial electrojet depend on the solar activity and a strong relationship exists between the two phenomena.

Chapter 1

Introduction

Our planet Earth has a thick outer envelop of gas, known as the atmosphere, which comprises dominantly neutral gases. Because the Earth is found inside the Sun's atmosphere, its neutral atmosphere is exposed to the stream of highly energetic radiations originated from the Sun. Especially solar radiations at ultraviolet (UV) and shorter X-ray wavelengths reach to the Earth's atmosphere carrying enormous energy. Absorption of photons of these wavelength ranges by the constituents of the neutral atmosphere, i.e, neutral atoms and molecules, causes dislodging of electrons from their outer most orbits. As a result of this process called photoionization, equal number of negatively charged particles (electrons) and positively charged particles (ionized atoms and molecules) are produced.

The Earths's upper atmosphere, which ranges from about 60 km altitude to $\frac{1}{3}$ of radius of the Earth, is a weakly ionized plasma called the Earth's ionosphere. Winds originated from various sources move the charged particles in the ionosphere across the geomagnetic field result in an electromotive force (emf) which then produces ionospheric current.

On 12th December 1901, Guglielmo Marconi demonstrated the first real long distance wireless radio communication between St. Johns, New Foundland, USA and Poldhu in the southern Tip of England, a distance of more than 3000 km across the Atlantic

ocean. At that time, it was known that except for very short distances, the radio waves did not follow the natural curvature of the Earth. Earth's curvature is a direct block to the line-of-sight communication. When enough distance separates the two radio stations so that their antennas fall behind the curvature, the Earth itself blocks the transmitted signals from the receiver. Marconi's success to this problem led Oliver Heaviside in England and A. E. Kennally in America, in 1902, to suggest that the radio waves must be reflected back to the Earth at considerable distances from the transmitter by a conducting charged layer in the atmosphere just as light rays are reflected from a mirror surface. Finally, in the year 1924 Appleton and Barnett in England, and Breit and Tuve in the U.S clearly demonstrated the existence of the ionosphere by recording echos from vertically transmitted radio waves [Richmond, 1995].

Solar radiation acting on the different constituents of the atmosphere generates layers or regions of ionization known by the letters D, E, and F. The D region is the inner most layer where the ionosphere starts covering the altitude range from about 60 to 90 km. The D region is associated with ionization by cosmic and X-rays and is not well understood. Recombination, which is the union of electrons with ions to establish a neutral atom or molecule, is very high in the D region. The E region is the middle layer, from about 90 km to 150 km above the surface of the Earth. Ionizations is due to soft X-ray (1-10nm) and far ultraviolet (UV) solar radiation ionizing oxygen atom (O), oxygen molecule (O_2) and nitrogen molecule (N_2). The primary ions are O_2^+ and NO^+. This region is also known as the Heaviside layer and the first to be discovered. At night the E layer begins to disappear because the primary source of ionization is no longer present. The F layers lie above 150 km altitude and are mainly dominated by O^+ ions. The lower, F_1, layer appears to be reasonably well understood, while the higher F_2 layer is not. At night the two layers, F_1 and F_2, unite. F region maximum is observed around 400 km. Extreme ultraviolet (EUV) is absorbed in this region.

Ionosphere is highly important for long distance communication by reflecting the radio waves back to Earth. Both radio and TV transmissions use radio waves. Since the dynamic changes taking place in the ionosphere affect our communication systems, understanding the physics of this region, therefore, is important to know the changes and design a method to improve our day today ways of communication.

The focus of this research is in the equatorial sector of the Earth's ionosphere because of two unique phenomena peculiar to this region, namely equatorial ionization anomaly and equatorial electrojet. The geometry of the geomagnetic field lines in the equatorial ionosphere is unique in such a way that the field lines are nearly horizontal. The nearly horizontal geomagnetic field lines combined with the eastward daytime electric field are believed to produce both phenomena.

Equatorial ionization anomaly is characterized as the occurrence of a trough in the ionization concentration at the equator and crests at about $\pm 20^0$ in magnetic latitude in each hemisphere [Appleton, 1946].

EIA is produced by equatorial fountain process which is driven by large scale electric field via $\vec{E} \times \vec{B}$, where $\vec{E}$ is the electric field and $\vec{B}$ is the magnetic field, drift [Rishbeth 2000, and references there in]. Numerical simulations of this process, including also electron production and loss and neutral air wind effect, have successfully reproduced the principal features of the anomaly (Baxter and Kendall, 1968; Abur-Robb and Windle, 1969; Sterling et al., 1969 (among others)).

Equatorial electrojet (EEJ), the second phenomena, is an intense daytime eastward electric current flowing in the E region of the ionosphere near the magnetic equator approximately between $\pm 2^0$ of the magnetic latitudes.

Using CHAMP Satellite's (Challenging Mini satellite Payload which is a German small satellite mission for geoscientific and atmospheric research and applications)

ion density and current profile data for the period 2000 to 2006, this thesis aims at understanding:

- latitudinal coverage of the EIA.
- longitudinal variation of the EIA.
- seasonal variation of the EIA.
- early evening characteristics of the EIA.
- relationship between the EIA and EEJ.

Organization of the thesis: The first chapter is introduction. The second chapter gives a brief theoretical and mathematical description about the Earth's ionosphere, EIA and EEJ. The third chapter presents some facts about the EIA obtained from CHAMP. The fourth chapter is about the relationship between EIA and EEJ. The last chapter is the conclusion and future work.

Chapter 2

Background

2.1 Earth's Ionosphere

The Earth's ionosphere is composed of large number of freely moving electrons, ionized atoms and molecules, and neutral gases. The number density of the ionospheric plasma have been observed to be as large as $10^{12}m^{-3}$ in the F region.

Photoionization is the major source of plasma production during the day. Plasma production rate diminishes rapidly after sunset since photo-ionization rate depends on the intensity of radiation absorbed. The solar radiation energy decreases in intensity as it penetrates deep toward the earth as a result of the radiation absorption by atmospheric constituents. On the contrary, neutral atmospheric density increases going down to the Earth. Because of these scenario, the ultraviolet and shorter wavelength components produce lesser plasma.

The plasma production rate also depends on rate of recombination reactions. Through recombination processes ions unite with electrons to reform the neutral gas. The recombination rate varies among the various constituents. For example, though the primary ions produced as a result of photo ionization process are N_2^+, O_2^+, N^+ and O^+, because of higher recombination rate of the nitrogen ions with the neutral gases, the nitrogen ions are rapidly converted to O_2^+ and NO^+ resulting in NO^+, O_2^+ and O^+ to be the dominant ions in the ionosphere. In the absence of photoionization

during the night, recombination decreases the plasma density.

2.1.1 Thermospheric Winds

Tidal wind fields are sources of ionospheric electric fields. Winds separate the ions and electrons, the separation is negated by production of polarization electric fields. Wind fields control the distribution of the electric fields and currents in the low and mid-latitude ionosphere.

Winds at ionospheric heights are generated mainly because of the diurnal variation in the absorption of solar UV radiation, which heats and expands the dayside thermosphere, ionospheric region above 90km altitude, creating day-to-night side horizontal pressure gradient. The wind created as a result of variation in pressure due to the variation in temperature blows from high to low pressure regions of the ionosphere. Horizontally directed winds dominate over vertical winds because of the fact that the atmosphere's much greater horizontal extent than vertical extent. Wind driven motions are, therefore, dominantly horizontal since vertical winds are small in magnitude and difficult to measure.

In the E region ionosphere, electrons and ions respond to winds differently. Electrons move hardly by the winds instead their motion is controlled by the electric fields and magnetic fields. On the other hand, ions move with the winds. The difference in response to the winds will result polarization of charges to build up and this generates ionospheric electric fields and then currents .

2.1.2 Forces acting on charged particles in the ionosphere

The main force fields controlling the motion of the ionospheric plasma are:

1. Electric fields: Any charged particle of charge q whether at rest or in motion experiences an electric force of $\vec{F} = q\vec{E}$ in the region of an electric field intensity $\vec{E}$. Electric fields are produced throughout a region in response to the requirement that the current generated by various forces be divergent free [R.A. Heelis,

2004]. The effects of polarization electric fields derived from neutral winds in one region and driving currents in all connected regions, have been examined by a number of investigators (Rishbeth, 1971b; Heelis et al., 1974; Farley et al., 1986; Haerendel and Eccles, 1992; Eccles, 1998a). The fundamental Physics describing the situation does not change; that is, the divergence of the total current must be zero.

2. The magnetic field: Magnetic field of intensity $\vec{B}$ exerts a force $\vec{F} = q(\vec{V} \times \vec{B})$ on any charge q whenever it tries to cross the region with velocity $\vec{V}$.

3. Collision Forces: During collision a momentum exchange force given by $\vec{F} = m\nu(\vec{V} - \vec{V}_n)$ is applied by collision frequency ν between charged particles of mass m and neutral particles. $\vec{V}$ is the velocity of the charged particles (electrons and ions) and $\vec{V}_n$ is the velocity of the neutral particles.

4. Pressure gradients: Any concentration gradient in plasma drives a plasma gradient of force $\vec{F} = \nabla(n\kappa_B T)$ which produces plasma motions in directions parallel and perpendicular to the magnetic field. n is the plasma number density, κ_B is Boltzmann's constant and T is the temperature. So, particles in plasma diffuse from high to low pressure gradient regions following the application of this force.

2.2 Equatorial Ionization Anomaly

Tropical region's (equatorial and low latitude regions) ionosphere shows an unusual plasma density distributions. The density of plasma in this region is minimum at magnetic equator (or dip equator) and there are two maxima on opposite sides of the magnetic equator. This phenomena is well known as **Equatorial Ionization Anomaly (EIA)**. The anomaly crest occurs from about $\pm 15^0$ to $\pm 20^0$ magnetic latitudes. The reason for the formation of the EIA structure is related to the equatorial fountain process, parallel pressure gradient and gravity.

The electric field in equatorial regions is usually directed eastward during the day

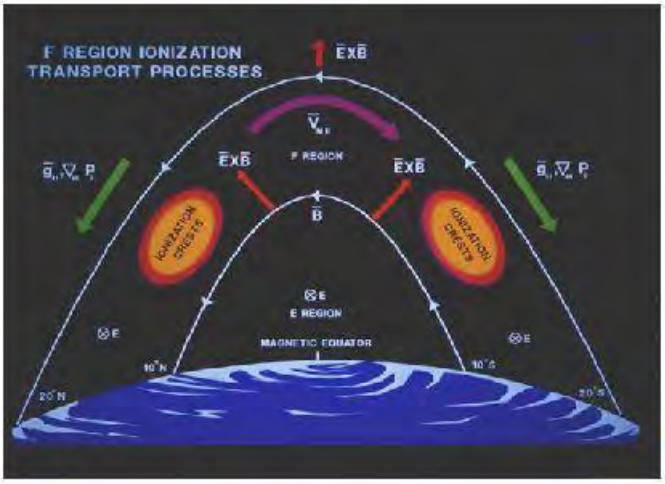

Figure 2.1: Schematic of the formation of the latitude variation of ionization density in the equatorial F region, known as the equatorial anomaly or the Appleton anomaly. The diagram illustrates that during daytime the eastward dynamo electric field from the E region maps along the magnetic field to F region heights above the magnetic equator. The plasma moves upward due to the $\vec{E} \times \vec{B}$ drift and then diffuses along the magnetic field to form two crests with maximum ionization density near $\pm 15^0$ magnetic latitude and minimum ionization at the magnetic equator.

time. The electric field in combination with the nearly parallel geomagnetic field at the dip equator causes the plasma to be lifted upward by $\vec{E} \times \vec{B}$ drift (Figure 2.1). The equatorial fountain process via the $\vec{E} \times \vec{B}$ drift tends to decrease the plasma density from the magnetic equator and move it to higher altitudes. The uplift of the plasma by the equatorial fountain process continues until the pressure gradient force field becomes strong enough. Then the plasma will be forced to move horizontally and downward by the horizontal pressure gradient and gravity along the magnetic field to form two crests with maximum ionization density near $\pm 15^0$ magnetic latitude. The $\vec{E} \times \vec{B}$ drift uplift both electrons and ions with the same velocity.

2.2.1 Velocity Equations

The charged particles in the Earth's ionosphere, electrons and ions, respond differently to the various force fields that act on them. The difference in mass between the ions and electrons plays an important role to the dynamical variations observed. As a result, relative motions are produced by the applications of external forces. The velocity equations derived below show the responses of electrons and ions in the Earth's ionosphere to the $\vec{E} \times \vec{B}$ drift at the magnetic equator.

Assumptions used: Neutrals and the various plasma species are considered as fluids that interact through collisions (multi fluid theory); the rate of change of the velocities of the systems is negligible. Under this assumption, the systems are in force equilibrium, i.e, the sum of the various forces acting on the ionospheric system are equal to zero. The pressure gradient and gravitational forces are neglected since they are not influential compared to Lorentz force and the frictional force. In addition to the above assumptions, above 90km all ion species are considered as singly ionized and have number density equal to that of the electrons [Richmond, 1995]. With these assumptions, the force equilibrium condition for ions and electrons can be put separately as:

$$n_e e(\vec{E} + \vec{V_i} \times \vec{B}) - n_e m_i \nu_{in}(\vec{V_i} - \vec{V_n}) - n_e m_i \nu_{ie}(\vec{V_i} - \vec{V_e}) = 0 \tag{2.2.1}$$

$$-n_e e(\vec{E} + \vec{V_e} \times \vec{B}) - n_e m_e \nu_{en}(\vec{V_e} - \vec{V_n}) + n_e m_e \nu_{ei}(\vec{V_i} - \vec{V_e}) = 0 \tag{2.2.2}$$

Where m_i and m_e are masses of the ion and electron, n_e is number density of the plasma, ν_{in} and ν_{en} are ion-neutral and electron-neutral collision frequencies, ν_{ie} and ν_{ei} are the collision frequencies between ions and electrons respectively. $\vec{V_i}$, $\vec{V_e}$ and $\vec{V_n}$ are ion, electron and neutral wind velocities, and $\vec{E}$ and $\vec{B}$ are the electric and magnetic fields respectively.

It is better to derive equation of motion of the ions first since the contribution of the collision term due to electrons on ions motion is less significant, because of the lighter mass of the electrons. Electron-ion collision frequency becomes significant in comparison to ion-neutral and electron-neutral only at very high altitudes in the F region. Ignoring this term, the perpendicular force equilibrium condition for the ions is given by

$$n_e e(\vec{E}_\perp + \vec{V_i} \times \vec{B}) - n_e m_i \nu_{in}(\vec{V_i} - \vec{V_n})_\perp = 0 \tag{2.2.3}$$

Dividing equation(2.2.3) by n_e and rearranging gives

$$e\vec{V_i} \times \vec{B} - m_i \nu_{in}(\vec{V_i} - \vec{V_n})_\perp = -e\vec{E}_\perp \tag{2.2.4}$$

Subtracting $e\vec{V_n} \times \vec{B}$ from both sides of Equation (2.2.4) yields the transformed equation of motion in a reference frame which moves with the neutral wind velocity $\vec{V_n}$.

$$e(\vec{V_i} - \vec{V_n}) \times \vec{B} - m_i \nu_{in}(\vec{V_i} - \vec{V_n})_\perp = -e(\vec{E}_\perp + \vec{V_n} \times \vec{B}) \tag{2.2.5}$$

Cross multiplication of Equation (2.2.5) by $\vec{B}$ and further simplification yields

$$-eB^2(\vec{V_i} - \vec{V_n})_\perp - m_i \nu_{in}(\vec{V_i} - \vec{V_n}) \times \vec{B} = -e(\vec{E}_\perp + \vec{V_n} \times \vec{B}) \times \vec{B} \tag{2.2.6}$$

Multiplying Equation (2.2.5) by $m_i \nu_{in}$ and Equation (2.2.6) by e and then adding them gives

$$m_i^2 \nu_{in}^2 (\vec{V_i} - \vec{V_n})_\perp + e^2 B^2 (\vec{V_i} - \vec{V_n})_\perp = m_i \nu_{in} e(\vec{E}_\perp + \vec{V_n} \times \vec{B}) + e^2 B(\vec{E}_\perp + \vec{V_n} \times \vec{B}) \times \hat{b}$$

where $\hat{b}$ is a unit vector in the direction of $\vec{B}$.

Rearranging yields

$$(m_i^2\nu_{in}^2 + e^2B^2)(\vec{V}_i - \vec{V}_n)_\perp = m_i\nu_{in}e(\vec{E}_\perp + \vec{V}_n \times \vec{B}) - e^2B\hat{b} \times (\vec{E}_\perp + \vec{V}_n \times \vec{B})$$

$$(\vec{V}_i - \vec{V}_n)_\perp = \vec{V}_{in\perp} = \frac{m_i\nu_{in}e(\vec{E}_\perp + \vec{V}_n \times \vec{B}) - e^2B\hat{b} \times (\vec{E}_\perp + \vec{V}_n \times \vec{B})}{(m_i^2\nu_{in}^2 + e^2B^2)}$$

$$\vec{V}_{in\perp} = \frac{m_i\nu_{in}eB(\vec{E}_\perp + \vec{V}_n \times \vec{B}) - e^2B^2\hat{b} \times (\vec{E}_\perp + \vec{V}_n \times \vec{B})}{Bm_i^2(\nu_{in}^2 + \frac{e^2B^2}{m_i^2})}$$

$$\vec{V}_{in\perp} = \frac{\nu_{in}\frac{eB}{m_i}(\vec{E}_\perp + \vec{V}_n \times \vec{B}) - (\frac{eB}{m_i})^2\hat{b} \times (\vec{E}_\perp + \vec{V}_n \times \vec{B})}{B(\nu_{in}^2 + (\frac{eB}{m_i})^2)}$$

$$\vec{V}_{in\perp} = \frac{\Omega_i\nu_{in}(\vec{E}_\perp + \vec{V}_n \times \vec{B}) - \Omega_i^2\hat{b} \times (\vec{E}_\perp + \vec{V}_n \times \vec{B})}{B(\nu_{in}^2 + \Omega_i^2)} \tag{2.2.7}$$

where $\Omega_i = \frac{eB}{m_i}$ is the gyro frequency of the ion.
Equation (2.2.7) is equation of motion for ions in the neutral wind frame.

Notice that the electron-ion collision term in electron's equation can not be neglected since electrons due to their lighter mass are easily deflected by collisions with ions. But, the inclusion of this term does bring significant change in the final result.

Following similar steps as has been done for ions above, the following results for electron can be obtained.

$$\vec{V}_{en\perp} = \frac{-\Omega_e\nu_{en\perp}(\vec{E}_\perp + \vec{V}_n \times \vec{B}) - \Omega_e^2\hat{b} \times (\vec{E}_\perp + \vec{V}_n \times \vec{B})}{B(\nu_{en\perp}^2 + \Omega_e^2)} \tag{2.2.8}$$

where $\Omega_e = \frac{eB}{m_e}$ is the gyro frequency of electron.

At high altitudes in the F region both electron and ion gyro frequencies become much larger than the corresponding collision frequencies (Richmond, 1995). That means

$$\Omega_i \gg \nu_{in} \tag{2.2.9}$$

and

$$\Omega_e \gg \nu_{en\perp} \tag{2.2.10}$$

Using the approximations in Equation (2.2.9) into Equation(2.2.7), we get

$$\vec{V}_{in\perp} = (\vec{V}_i - \vec{V}_n)_\perp = -\frac{\hat{b} \times (\vec{E}_\perp + \vec{V}_n \times \vec{B})}{B} = \frac{\vec{E}_\perp \times \hat{b}}{B} - \vec{V}_n \tag{2.2.11}$$

Hence, the perpendicular component of the ion velocity is given by

$$\vec{V}_{i\perp} = \frac{\vec{E}_\perp \times \hat{b}}{B} \tag{2.2.12}$$

Using the approximations in Equation (2.2.10) into Equation (2.2.8), the velocity of electron in the moving frame becomes

$$\vec{V}_{en\perp} = (\vec{V}_e - \vec{V}_n)_\perp = -\frac{\hat{b} \times (\vec{E}_\perp + \vec{V}_n \times \vec{B})}{B} = \frac{\vec{E}_\perp \times \hat{b}}{B} - \vec{V}_n \tag{2.2.13}$$

Hence, the perpendicular component of the electron velocity is given by

$$\vec{V}_{e\perp} = \frac{\vec{E}_\perp \times \hat{b}}{B} \tag{2.2.14}$$

Comparing Equation (2.2.12) and (2.2.14), we see that

$$\vec{V}_E = \vec{V}_{i\perp} = \vec{V}_{e\perp} = \frac{\vec{E}_\perp \times \hat{b}}{B} = \frac{\vec{E}_\perp \times \vec{B}}{B^2} = \frac{(\vec{E}_\parallel + \vec{E}_\perp) \times \vec{B}}{B^2} = \frac{\vec{E} \times \vec{B}}{B^2} \tag{2.2.15}$$

since $\vec{E}_\parallel \times \vec{B} = 0$.
Equation (2.2.15) shows that both electrons and ions drift upward with the same velocity by $\vec{E} \times \vec{B}$ drift.

Using the known values, 0.25G and 0.5mV/m for the magnetic intensity at magnetic equator and electric field intensity respectively, by $\vec{E} \times \vec{B}$ drift both electrons and ions move upward from magnetic equator at an average velocity of 20m/s during the

day time. This value increases dramatically during the pre reversal periods to 40m/s.

Subtracting Equation (2.2.8) from (2.2.7) and multiplying the result by $n_e e$ gives the current density perpendicular to the magnetic field.

$$\begin{aligned}\vec{J}_\perp &= \frac{n_e e}{B}\left(\frac{\nu_{in}\Omega_i}{\nu_{in}^2+\Omega_i^2}+\frac{\nu_{en\perp}\Omega_e}{\nu_{en\perp}^2+\Omega_e^2}\right)(\vec{E}_\perp+\vec{V}_n\times\vec{B}) \\ &+ \frac{n_e e}{B}\left(\frac{\Omega_e^2}{\nu_{en\perp}^2+\Omega_e^2}-\frac{\Omega_i^2}{\nu_{in}^2+\Omega_i^2}\right)\hat{b}\times(\vec{E}_\perp+\vec{V}_n\times\vec{B}) \qquad (2.2.16)\end{aligned}$$

$$\vec{J}_\perp = \sigma_P(\vec{E}_\perp+\vec{V}_n\times\vec{B})+\sigma_H\hat{b}\times(\vec{E}_\perp+\vec{V}_n\times\vec{B}) \qquad (2.2.17)$$

where

$$\sigma_P = \frac{n_e e}{B}\left(\frac{\nu_{in}\Omega_i}{\nu_{in}^2+\Omega_i^2}+\frac{\nu_{en\perp}\Omega_e}{\nu_{en\perp}^2+\Omega_e^2}\right) \qquad (2.2.18)$$

is called the Pedersen conductivity and

$$\sigma_H = \frac{n_e e}{B}\left(\frac{\Omega_e^2}{\nu_{en\perp}^2+\Omega_e^2}-\frac{\Omega_i^2}{\nu_{in}^2+\Omega_i^2}\right) \qquad (2.2.19)$$

is the Hall conductivity.

The parallel component of the current density, on the other hand, can be obtained from Equation (2.2.1) and (2.2.2) following similar techniques and using $\frac{m_e}{m_i}\approx 10^{-5}$, though this value depends on the ions compositions, and $\frac{\nu_{en}}{\nu_{in}}\approx 10$ [Richmond, 1995].

$$\vec{J}_\parallel = n_e e(\vec{V}_i-\vec{V}_e)_\parallel \qquad (2.2.20)$$

$$\vec{J}_\parallel = \frac{n_e e^2\vec{E}_\parallel}{m_e(\nu_{en\parallel}+\nu_{ei\parallel})} = \sigma_\parallel\vec{E}_\parallel \qquad (2.2.21)$$

where

$$\sigma_\parallel = \frac{n_e e^2}{m_e(\nu_{en\parallel}+\nu_{ei\parallel})} = \frac{n_e e^2}{m_e\nu_e} \qquad (2.2.22)$$

$\sigma_\parallel$ (or σ_0) is called the parallel conductivity.

Adding Equations (2.2.16) and (2.2.21) gives the well known **Ampere's law** that relates the current density vector with the conductivities.

2.3 Equatorial Electrojet

Daytime electrodynamics of the ionosphere is strongly controlled by the E region. This is because of the fact that there is high density ionizable neutral gas combined with enough ionizing solar UV and X-ray radiation as a result the region posses higher conductivity than the other regions in the day.

During the daytime, the zonal component of the electric field produced by tides due to solar heating is usually eastward. This electric field is amplified and causes an intense eastward electric current near magnetic equator, better known as equatorial electrojet(EEJ). The equatorial electrojet flows in the E region of the equatorial ionosphere where the dip angle is small.

The daytime zonal electric field drives a small eastward Pedersen current and downward Hall current. The conductivity profiles show that the Hall conductivity dominates over Pedersen in the E region below about 120km altitudes. In addition, the Hall conductivity vanishes near the boundaries of the E region. As a result, Hall current is not allowed to cross the boundaries and charge begins to accumulate near the boundaries resulting in polarization of charges (Figure 2.2). This produces a strong vertically upward polarization electric field in order to satisfy the requirement of free current density in the vertical direction. The vertical polarization field drives an upward Pedersen current to counter balance the downward Hall current. This equalizing upward Pedersen current makes the vertical direction divergence free and maintains current continuity requirement. The stronger vertical polarization electric field, Equation (2.3.5), will also drive large electric current to the east direction.

The current density, $\vec{J}$, is given by

$$\vec{J} = \hat{\sigma} \cdot \vec{E} \tag{2.3.1}$$

where the conductivity tensor $\hat{\sigma}$ at the magnetic equator is given by

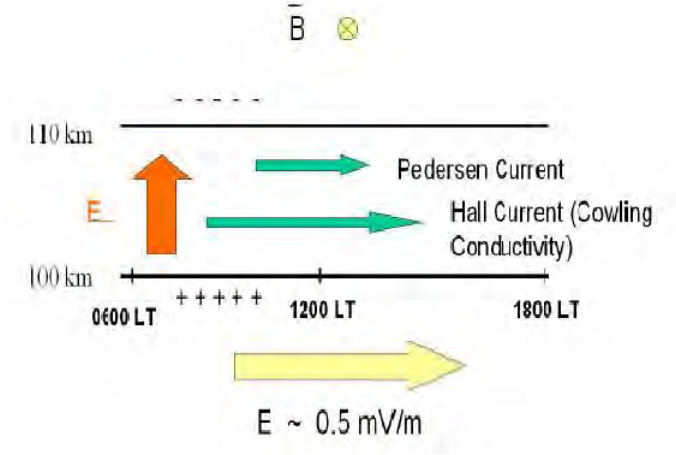

Figure 2.2: Equatorial electrojet in a slab geometry.

$$\begin{pmatrix} \sigma_P & 0 & \sigma_H \\ 0 & \sigma_0 & 0 \\ -\sigma_H & 0 & \sigma_P \end{pmatrix} \tag{2.3.2}$$

The horizontal and vertical components of the current density vector are given by

$$J_x = \sigma_P E_x + \sigma_H E_z \tag{2.3.3}$$

$$J_z = -\sigma_H E_x + \sigma_P E_z \tag{2.3.4}$$

From (2.3.4) we can see that the vertical, E_z, electric polarization field should be very large as compared to the original eastward electric field, E_x, since $\sigma_H > \sigma_P$ in the E region and since vertical current is assumed to be suppressed, i.e $J_z \simeq 0$. Hence,

$$J_z = -\sigma_H E_x + \sigma_P E_z = 0$$

$$E_z = \frac{\sigma_H}{\sigma_P} E_x \tag{2.3.5}$$

Substituting(2.3.5) to (2.3.3) we get

$$J_x = \sigma_P E_x + \sigma_H (\frac{\sigma_H}{\sigma_P}) E_x$$

$$J_x = (1 + \frac{\sigma_H^2}{\sigma_P^2}) \sigma_P E_x = \sigma_C E_x \tag{2.3.6}$$

where $\sigma_C = (1 + \frac{\sigma_H^2}{\sigma_P^2})\sigma_P$ is the so called Cowling conductivity. In this calculation, the local neutral wind does not involve at all for simplicity and the electrojet is set up by the global tidal winds that create the diurnal zonal electric field component measured at the equator. Additionally, since the cross product of the meridional component of the wind with the magnetic field vanishes at the magnetic equator, this component does not enter into the calculation. Equation (2.3.6) shows that the zonal conductivity is enhanced by the large Cowling conductivity factor, $1 + \frac{\sigma_H^2}{\sigma_P^2}$ with an estimated value of 100, producing an intense eastward electric current at the equator, known as the equatorial electrojet, during the daytime.

Chapter 3

Equatorial Ionization Anomaly derived from CHAMP Satellite

THE CHAMP SATELLITE

CHAMP (Challenging Mini satellite Payload) is a German small satellite mission for geoscientific and atmospheric research and applications. With its highly precise, multifunctional and complementary payload elements (magnetometer, accelerometer, star sensor, GPS receiver, laser retro reflector, ion drift meter) and its orbit characteristics (near polar, low altitude, long duration), CHAMP generates simultaneously highly precise gravity and magnetic field measurements over five years period. This will allow to detect besides the spatial variations of both fields also their variability with time.

The CHAMP satellite was launched from the cosmodrome Plesetsk (north of Moscow) aboard a Russian COSMOS launch vehicle into an almost circular, near polar (inclination = 87^0) orbit with an initial altitude of 454 km on July 15, 2000 at 11:59:59.628 UTC. The reason for choosing an almost circular and near-polar orbit is the advantage of getting a homogeneous and complete global coverage of the Earth's sphere with orbit and magnetometer measurements.

State Vector for CHAMP

- epoch = 2000/08/01 00:00:00 GPS
- semi major axis = 6823.287 km
- eccentricity = 0.004001
- inclination = 87.277 deg
- argument of perigee = 257.706 deg
- true period = 93.55 min
- rev/day = 15.40
- perigee period = 93 days

Based on seven years of CHAMP data (2000 to 2006), the variation in the plasma density, n_e, in the EIA structure with latitude, longitude, seasons and early evening characteristics are described below.

1. Latitudinal coverage:

Figure 3.1 shows the noon time latitudinal coverage of the equatorial ionization anomaly structure for 95^0 longitude for March (2001-2006). As can be seen from this figure, the anomaly has a minimum plasma density, about $5.0 \times 10^{11} m^{-3}$, at the dip equator in March 13, 2004. Sandwiched between the two maximum density peaks, with values about $3.5 \times 10^{12} m^{-3}$ in March 21, 2001. The minimum density observed at the dip equator for all cases in Figure 3.1 is produced due to the removal of the plasma via the equatorial fountain process. The equatorial fountain process via $\vec{E} \times \vec{B}$ drift pushes the plasma to higher altitudes, ranging from few hundreds to few thousand kilometers, in effect diminishing the plasma density at the dip equator. The upward motion of the plasma continues until the pressure gradient force becomes

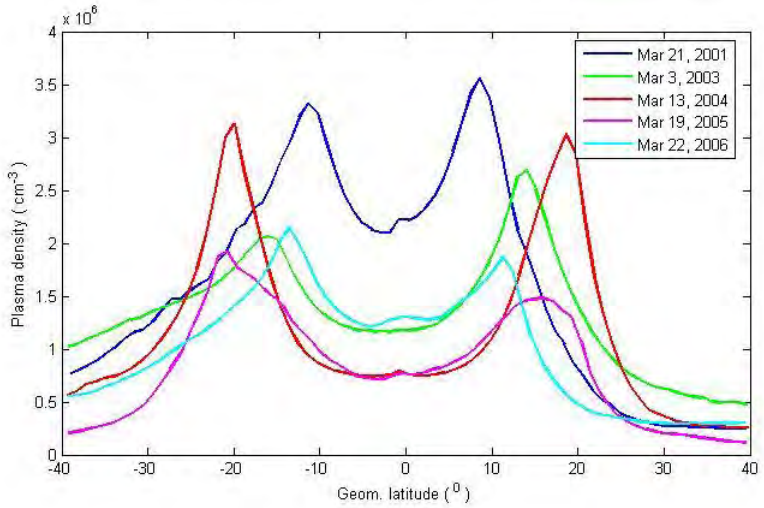

Figure 3.1: Shows how the equatorial ionization anomaly structure varies with latitude near Pacific (95^0 east longitude)

strong enough to block the uplift by the equatorial fountain process.

The plasma removed from the dip equator to higher altitudes is then forced to move horizontally and downward to higher latitudes to both hemispheres because of the transport mechanisms by diffusion and gravity to create the anomaly peaks from $\pm 10^0$ to $\pm 20^0$ latitudes (Figure 3.1). In times when the fountain process is not strong to remove large amount of plasma from the dip equator as in the blue curve, the anomaly depth will be shallow and the plasma density near the dip equator will be relatively large. On the other hand, if the fountain process is strong, the plasma density at the dip equator will be swept to very low values, as compared to the peak values, and the depth of the anomaly will be very wide, as in the red curve.

2. Longitudinal variation:

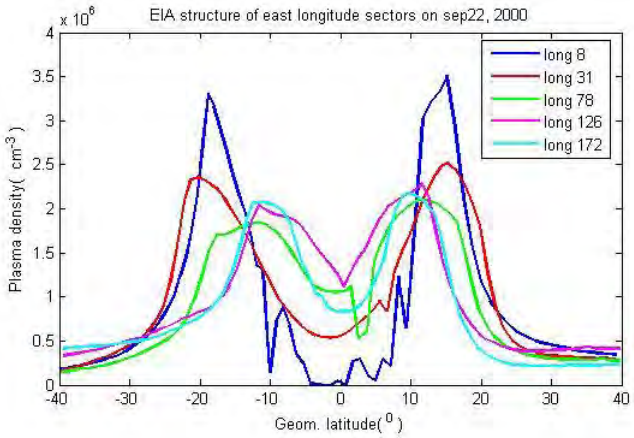

Figure 3.2: EIA structures to the east of the Greenwich Meridian on September 22, 2000.

Noon time equatorial ionization anomaly structures of September 22, 2000 for longitudes to the east and west of the Greenwich meridian are plotted in Figure 3.2 and Figure 3.3. The eastern longitude curves (Figure 3.2) reveal that there exists variation in the anomaly structure, although it is not that much significant as compared to the western ones. The blue curve in Figure 3.2 shows the anomaly structure for longitude 8^0 east. This curve indicates that the anomaly trough is exactly at the dip equator and the anomaly structure is distorted somewhat from the normal. The distortion might be caused by the plasma transport due to local winds. In addition, the anomaly for the blue curve posses the maximum plasma density, as compared to the other curves in the same figure, the crest regions have density values approximately about $3.5 \times 10^{12} m^{-3}$ at about $\pm 20^0$. Furthermore, the blue and red curves show that the anomaly structure for longitudes 8^0 and 31^0 east, respectively, are wider than the other longitude sectors. This may suggest the presence of strong fountain process and driver electric fields in these longitude sectors. One thing that all the curves posses

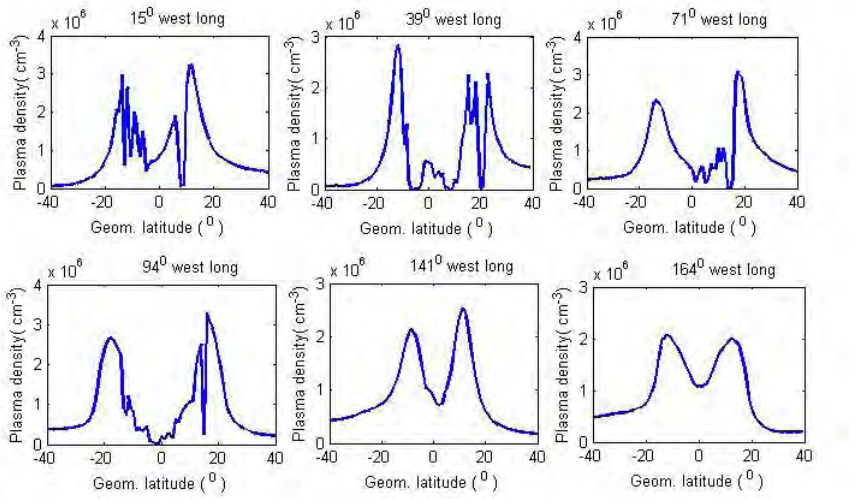

Figure 3.3: EIA structures to the west of the Greenwich Meridian on September 22, 2000.

in common is that the symmetry in the anomaly structure between the northern and southern hemispheres.

Western longitude anomaly curves of Figure 3.3 show that the anomaly structures for longitudes between the Greenwich Meridian and 100^0 have irregularity in the plasma density distribution and even split in the anomaly structure. Transequatorial winds might moved the plasma to various directions to affect the smooth nature of the anomaly structure to yield anomaly structures like that of Figure 3.3. Recombination processes might also plays a role in this EIA structure formation. The anomaly curves in longitudes 141^0 and 164^0 west are normal anomaly structures with their trough located at the dip equator as usual and the peaks at about $\pm 15^0$ latitudes.

3. Seasonal variation:

The 3D plots shown in Figure 3.4 to 3.7 indicate how the anomaly structure varies

through out the year 2001 in the pacific longitude sector (75^0 west) during the day time between 10:00 and 17:00LT. These graphs clearly show the existence of daily, seasonal and latitudinal variation in the anomaly structure. For example, Figure 3.4 shows how the EIA varies during the three months February, March and April. The anomaly structure as can be observed from this figure exhibits minimum plasma density at the dip equator with value approximately $1.5 \times 10^{12} m^{-3}$, though this value shows a slight day-to-day variation. However, the anomaly values in the crest regions vary greatly from day to day compared to the trough values and the crest region values show greater increase between the last week of March and the first week of April, red colored region. The locations of the northern and southern crests also show variation from $\pm 15^0$ to $\pm 20^0$ during the three months. The maximum crest plasma density value observed on April 8 at 14:00LT was about $5.0 \times 10^{12} m^{-3}$. This value was not seen through out the year 2001 in the pacific longitude sector. In addition, the anomaly structure in most of the curves during the three months exhibits symmetry. The asymmetry observed in some of the curves might be caused by the presence of local winds and inhomogeneous heating and ionization of the atmosphere by the Sun.

Figure 3.5, on the other hand, shows the anomaly structure during the months May, June and July 2001. The plasma density in both crest and trough regions shows continuous decrement from May to July as can be observed from Figure 3.5. Minimum crest density value, asymmetry and narrow depth in the anomaly structure are the characteristics of the anomaly here. The narrowness in the depth of the anomaly may be related to the strength of the fountain process. We know that if the fountain process is weak, the plasma will not be pushed to very high altitudes and so through the action of pressure gradient and gravity forces moves down along the magnetic field lines away from dip equator but to near latitudes. The anomaly structure in these months possessed the least plasma density in the anomaly crest regions compared to the other months of the same year. The Photoionization process is stronger in the northern hemisphere than the southern hemisphere during these months, because the Sun spends most of the time in this hemisphere during these months. So, there exists

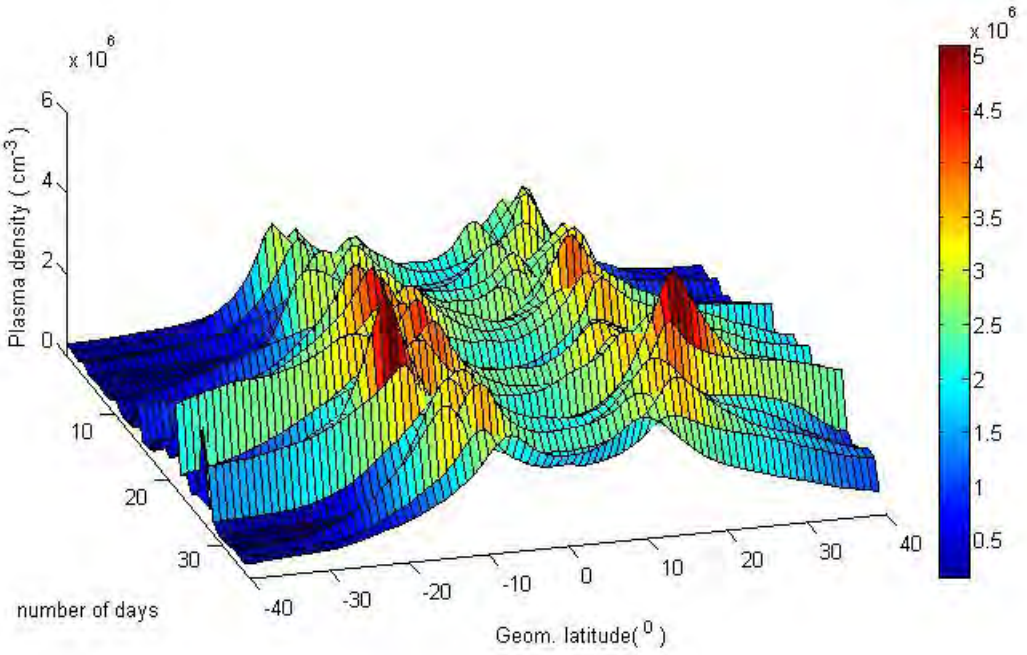

Figure 3.4: Equatorial ionization anomaly structure of the Pacific longitude sector (75^0 west) for the three months February, March and April 2001.

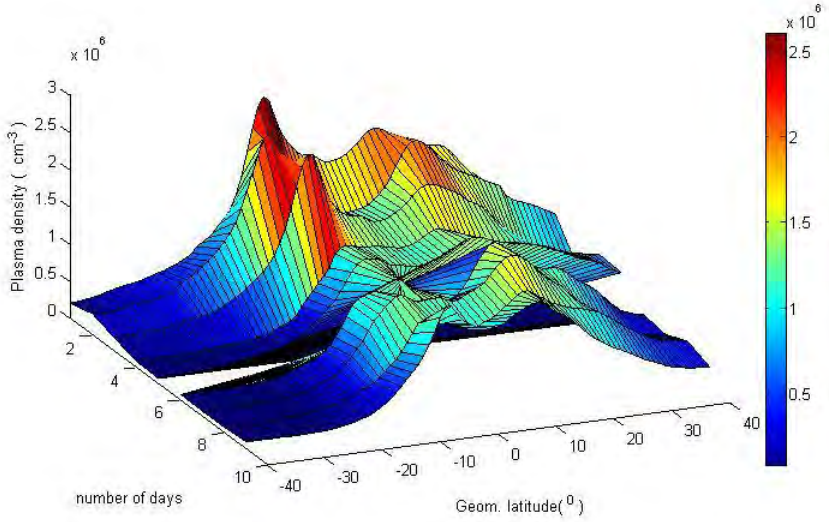

Figure 3.5: Equatorial ionization anomaly structure of the Pacific (75^0 west longitude) for the three months May, June and July.
2001.

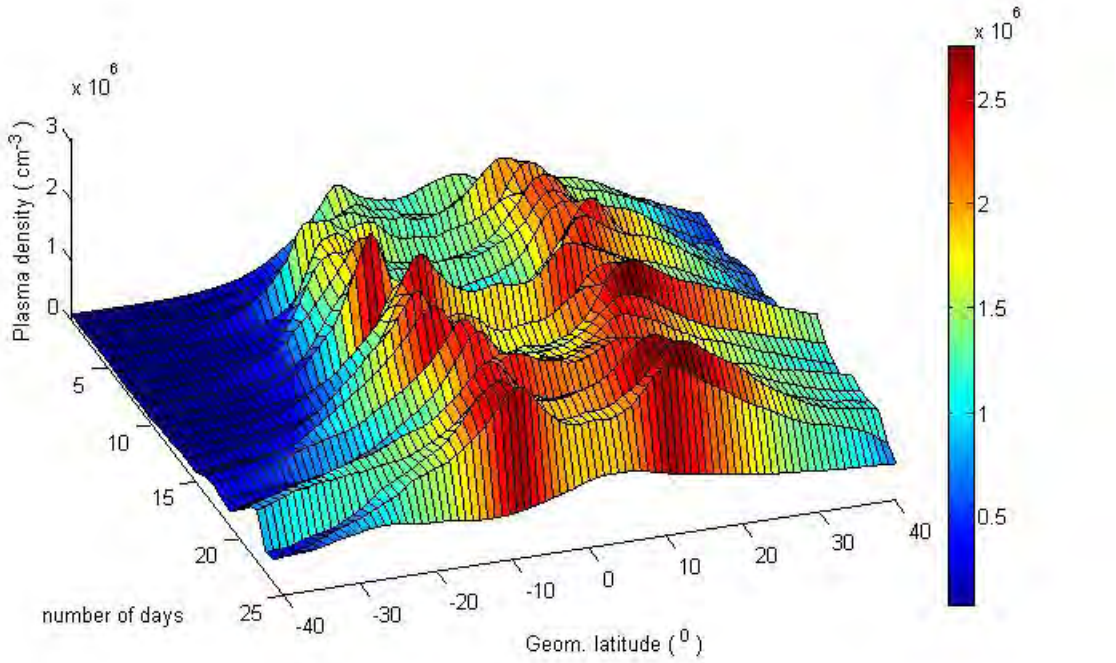

Figure 3.6: Equatorial ionization anomaly structure of the Pacific (75^0 west longitude) for the three months August, September and October 2001.

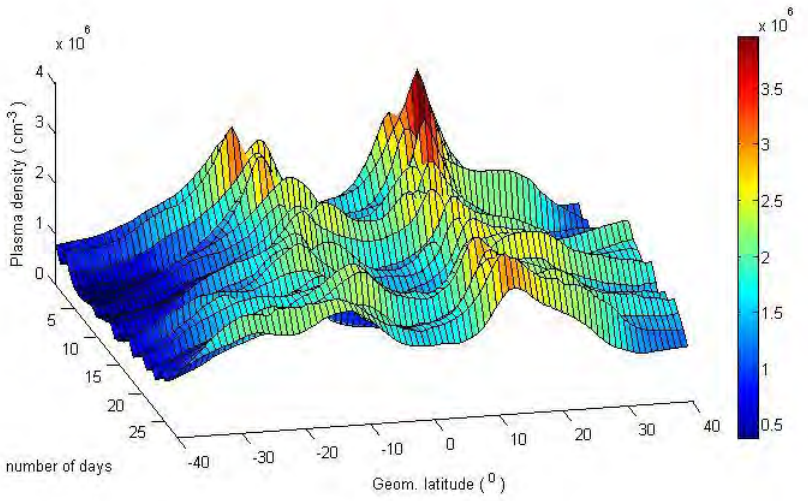

Figure 3.7: Equatorial ionization anomaly structure of the Pacific (75^0 west longitude) for the three months November 2001 to January 2002.

plasma gradient due to this reason. The eruption of pressure gradient force field assisted by winds drives the plasma to the southern hemisphere to produce asymmetry.

Figures 3.6 and 3.7 show how the anomaly structure varies in the remaining seasons of the same year. The symmetry in the anomaly structure is highest for the months of August to October as can be seen from Figure 3.6. The crest density values show variation between $1.5 \times 10^{12} m^{-3}$ and $3.0 \times 10^{12} m^{-3}$ which is slightly lower (in value) than the months February, March and April. However, in the latter case the anomaly crest density values show greater variation during the three months.

Observation of Figure 3.7 indicates that the anomaly, during the months November and December 2001 and January 2002, has asymmetry, with more plasma density in the northern hemisphere than the south, the trough region has moved from the dip equator slightly to the northern hemisphere. Similar reasoning can be put forward for these observations as for Figure 3.5.

4. Early evening characteristics of the equatorial ionization anomaly

Near the evening hours (between 18:00 and 19:00 LT), the ionosphere is lifted up considerably after sunset by increasing upward plasma drifts related to the prereversal enhancement of the eastward electric field [e.g., Abdu, 2001, and references there in]. The degree of uplift positively depends on the prereversal enhancement, whose magnitude has been shown by Fejer et al.[1995] to increase with solar cycle, particularly near the equinox and December solstice. The evening enhancement of the vertical velocity (eastward electric field) is a direct consequence of the considerably more rapid decrease of the E region conductivity after sunset compared to that of the F region. This pre-reversal enhancement in the eastward electric field causes the equatorial fountain to increase dramatically to very high magnitudes which consequently removes large amount of plasma from the dip equator to very high altitudes (more than 1000 km) to create large amount crest region plasma densities as can be

seen in Figure 3.8. The crest region plasma density exceeds 30 to 40 times than that of the trough region plasma density. Figure 3.8 clearly shows this fact for a single day observation on September 2000 for fifteen longitude sectors.

The curves colored with blue indicate what the anomaly structure looked on that day for the west longitude sectors, west of the Greenwich Meridian, and the reds for the eastern, east of the Greenwich Meridian. In all cases except for the blue curve of longitude 45^0 west, the troughs of the anomalies, as usual, were located at the dip equator. The anomaly at 45^0 west longitude as a whole was moved to the northern hemisphere so as to create the southern anomaly crest near 10^0 longitude and the northern anomaly crest near 30^0 longitude and the trough near 10^0 east. The reason might be the presence of strong equatorward winds from the southern hemisphere to drive the plasma to the northern hemisphere. The difference between the eastern and western anomaly structures for all other paired curves might be caused by the strength of the fountain process and solar ionization.

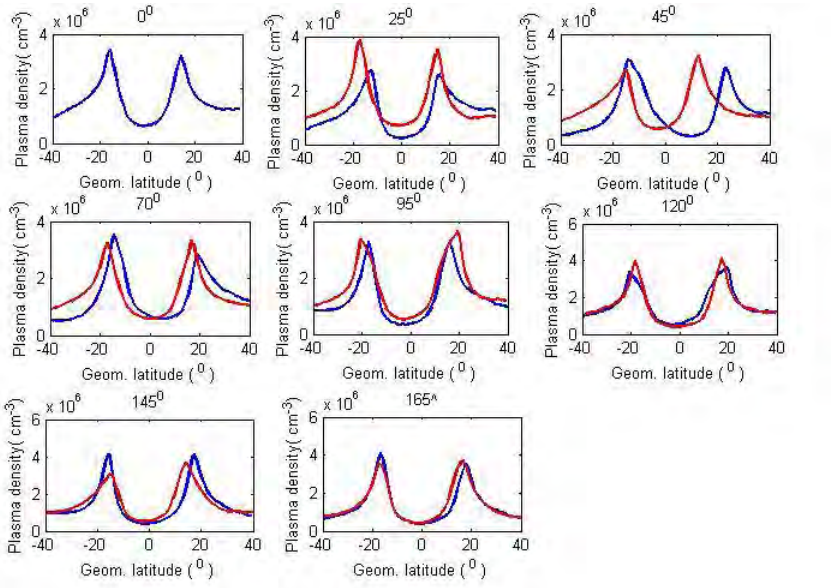

Figure 3.8: Equatorial ionization anomaly structures during the pre-reversal hours of March 21, 2002 for fifteen longitude sectors.

Chapter 4

Equatorial Electrojet and Equatorial Ionization Anomaly from CHAMP Satellite

The equatorial electrojet and equatorial ionization anomaly are both a consequence of the dynamic equatorial plasma processes. They are driven by equatorial zonal electric fields. In the following section we will see how the two phenomena are related using CHAMP satellite's current profiles and ion density data.

1. EEJ and EIA structures near solar maximum (2000) and solar minimum (2006)

Figures 4.1 to Figure 4.4 show EEJ and EIA structures near solar maximum and solar minimum conditions. These graphs show that the EIA and EEJ undergo significant changes indicating that both plasma processes are related with the sunspot numbers.

In Figure 4.1, we see that the EEJ develops between about $\pm 2^0$ magnetic latitudes. But the EEJ maximum is seen exactly at the dip equator for both cases (December 2000 and 2005) with value about 0.05 A/m. Although there was no significant difference between the two EEJ current profiles, the anomaly structures show great discrepancy between the two years. This fact may indicate that a small change in current can be caused by polarizing electric fields which could give rise to fountain process to having a remarkable difference in the crest density values.

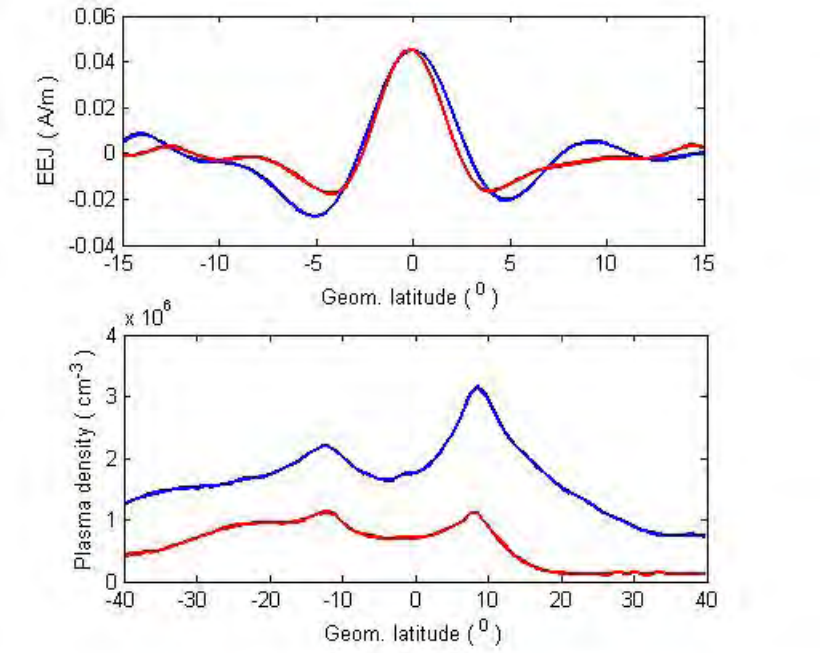

Figure 4.1: Shows the EEJ structure in December 2000 and 2005 by the blue and red colors respectively (top figure) and the EIA structure for the corresponding curves (bottom figure) near Addis Ababa (39^0 east longitude)

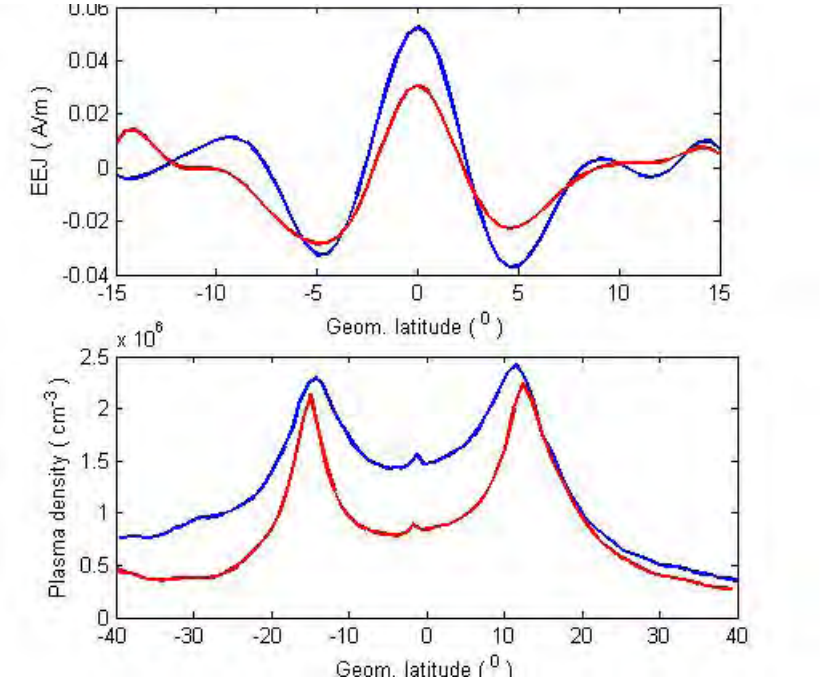

Figure 4.2: Shows the EEJ structure in March 2003 and 2005 by the blue and red colors respectively (top figure) and the EIA structure for the corresponding curves (bottom figure) near Addis Ababa (39^0 east longitude)

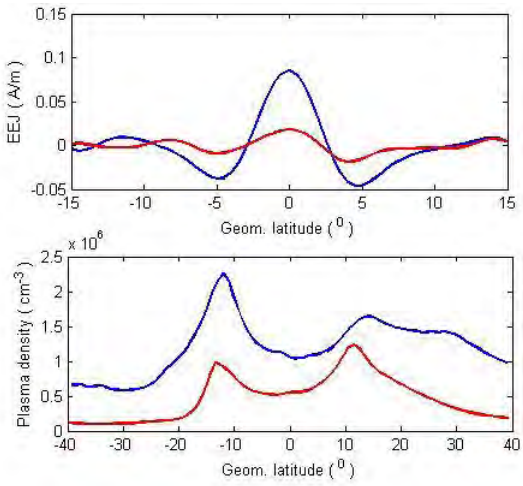

Figure 4.3: Shows the EEJ structure in June 2002 and 2006 by the blue and red colors respectively (top figure) and the EIA structure for the corresponding curves (bottom figure) near Addis Ababa (39^0 east longitude)

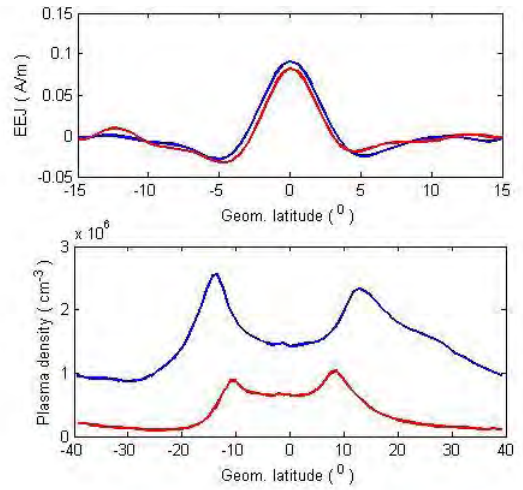

Figure 4.4: Shows the EEJ structure in September 2001 and 2006 by the blue and red colors respectively (top figure) and the EIA structure for the corresponding curves (bottom figure) near Addis Ababa (39^0 east longitude)

Figure 4.2 and Figure 4.3 show the existence of strong correlation between EEJ and EIA phenomena. In these figures, EEJ structures deviate significantly during the two years we are making a comparison. EEJ values near the solar maximum, blue colors, are greater than those near the solar minimum, red colors. Since the measurements were made atmost at the same time for both cases, the difference might be caused by the difference in the solar activity. The effect in the EIA structure for both cases can be seen in the bottom figures. EIA structures in Figure 4.2 and Figure 4.3 show that the plasma density values for both crest and trough near the solar maximum are greater than those near the solar minimum. So, we might conclude from these two figures that an increase in the EEJ magnitude could cause an increase in the plasma density value in the anomaly structure.

Figure 4.4, on the other hand, shows the appearance of EEJ and EIA structures for September 2001 and 2006. As in Figure 4.1, the EEJ values in this figure also show a small deviation. However, the EIA structures for the corresponding times that the anomaly structures has significant separation between September 2001 and 2006.

In general, Figures 4.1 to 4.4 suggest that the F region EIA structure possesses greater plasma density values when there is a stronger EEJ flowing in the E region of the ionosphere.

2. Seasonal variations of EEJ and EIA structures

In the previous chapter, we have seen that the equatorial ionization anomaly structure shows seasonal variation. In this section we will see how the equatorial electrojet and equatorial ionization anomaly vary with season.

Figure 4.5 (for December 2001) shows that both EEJ and EIA exhibit day-to-day variation. The maximum EEJ value as can be observed from the graph is about 0.1 A/m and that of the EIA crest plasma density value is about $3.5 \times 10^{12} m^{-3}$. The

reason for the day-to-day variation might be due to the variation in the solar heating and recombination processes.

Figure 4.6 shows structures of EEJ and EIA during June 2002 in Addis Ababa (39^0 east longitude). The EEJ graph indicates that though there are day-to-day variations, there was a general decrease in the magnitude of the current going to July. Similarly, the anomaly structures exhibits day-to-day variation showing decrease towards the last week of June. The maximum current and crest plasma density values observed were about 0.1 A/m and $3.0 \times 10^{12} m^{-3}$ respectively. The two graphs indicate that there exists a relationship in terms of driven between the two phenomena, the EEJ and the EIA.

Figure 4.7 shows the EEJ and EIA structures in September 2002 in the Addis Ababa (39^0 east longitude). For this season too, both EEJ and EIA phenomena possessed day-to-day variation. The maximum value of current and crest plasma density values can be seen from the figures was about 0.15 A/m and $3.5 \times 10^{12} m^{-3}$. The maxima were seen in the first week of September 2002.

Figure 4.8 clearly shows the relationship between EEJ and EIA. The EEJ graph shows that the current density was maximum in the first week of March 2003 near Addis Ababa . The current density decreases going to the last week of March 2003. The maximum current density value observed was about 0.1 A/m and the the anomaly crest plasma density value was $2.5 \times 10^{12} m^{-3}$.

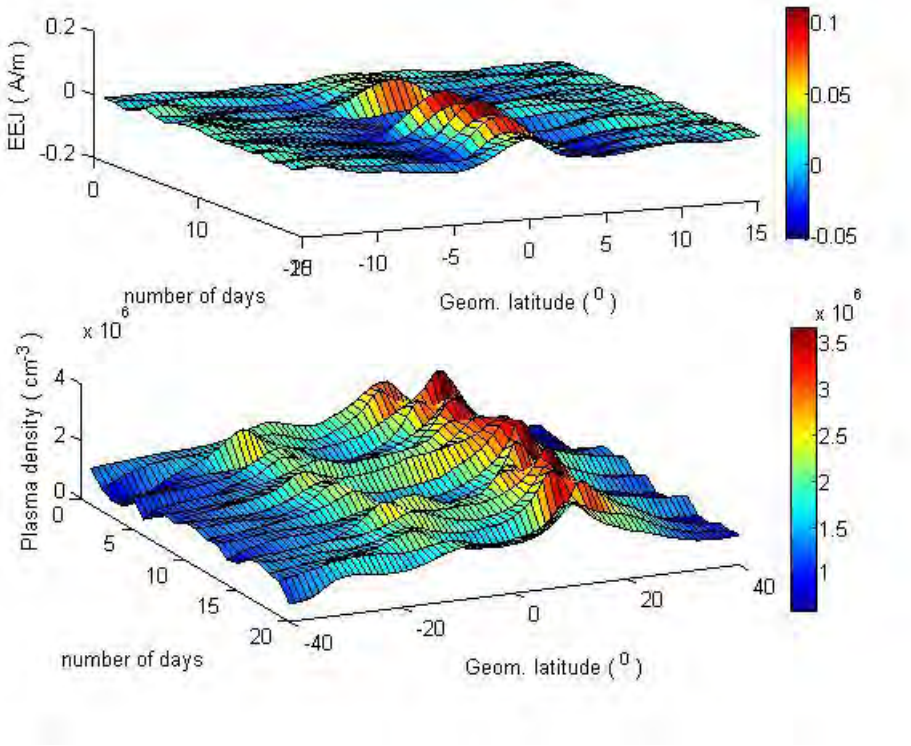

Figure 4.5: Shows the equatorial electrojet and equatorial ionization anomaly structures of December 2001 in Addis Ababa (39^0 east longitude)

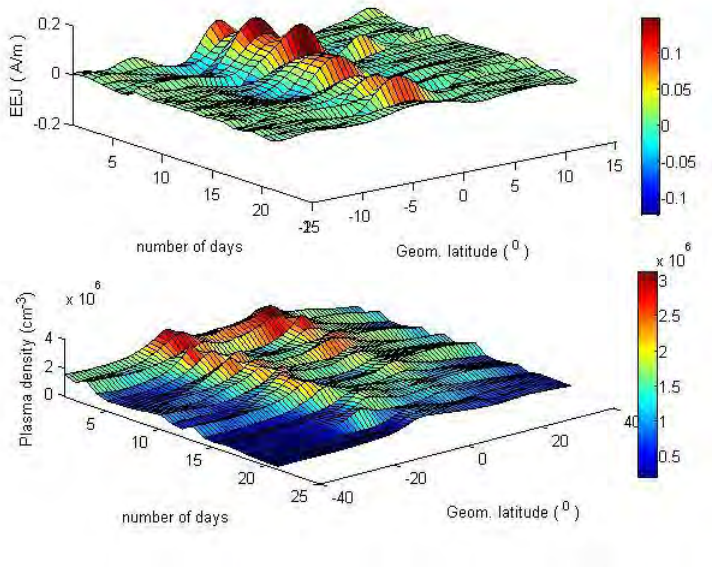

Figure 4.6: Shows the equatorial electrojet and equatorial ionization anomaly structures of June 2002 in Addis Ababa (39^0 east longitude)

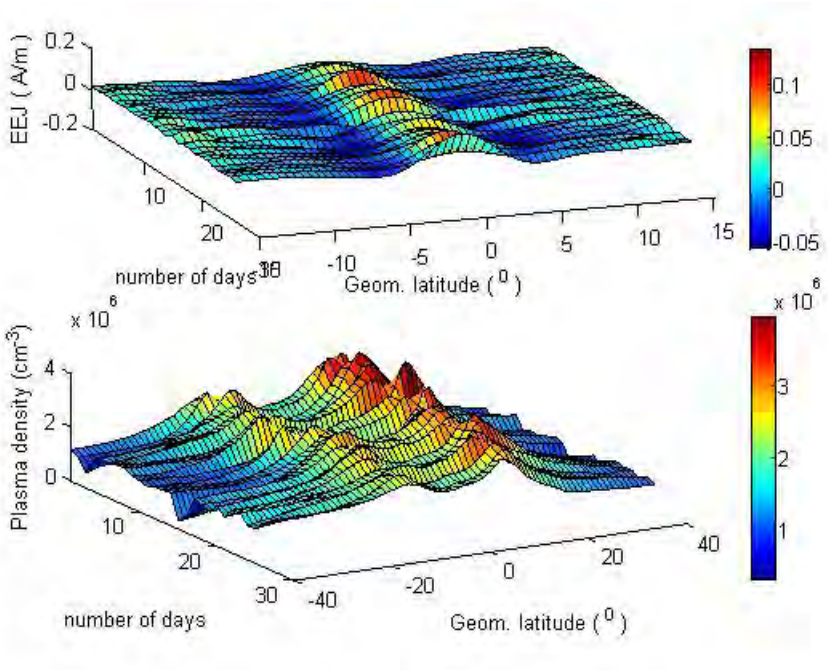

Figure 4.7: Shows the equatorial electrojet and equatorial ionization anomaly structures of September 2002 in Addis Ababa (39^0 east longitude)

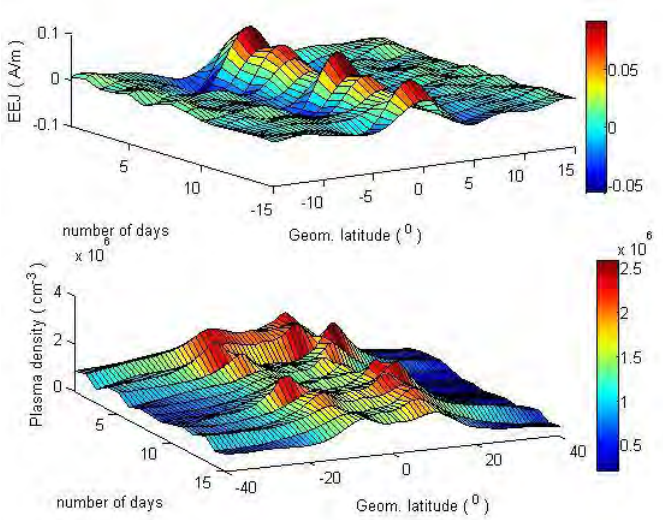

Figure 4.8: Shows the equatorial electrojet and equatorial ionization anomaly structures of March 2003 in Addis Ababa (39^0 east longitude)

Chapter 5

Conclusion And Future Work

Equatorial ionization anomaly is a strange plasma density distribution with minimum plasma density located at the magnetic equator in between two maximum plasma density peaks at about $\pm 20^0$ in opposite sides of the magnetic equator. Equatorial electrojet, on the other hand, is an intense electric current flowing in the E region of the ionosphere. They are driven by equatorial zonal electric fields.

In this thesis we have found out that

1. EIA varies rapidly with latitude as well as longitude.
2. The anomaly structure shows stronger symmetry near September and asymmetry near June.
3. The plasma density structure in the EIA exhibits a day-to-day and seasonal variation.
4. Anomaly structures near the evening hours show that the plasma density at the trough will be drastically minimized and the crest plasma density value is increased one to two orders of magnitude than the noon time crest density values. This is because of the reversal enhancement of the zonal electric fields.
5. Both equatorial electrojet and equatorial ionization anomaly phenomena depend on the solar activities. Both processes tend to decrease from solar maximum to solar minimum.

6. There exists a strong relationship between EEJ and EEIA. The stronger the EEJ current, the stronger the equatorial eastward electric field and results in a stronger equatorial plasma fountain and EIA [Sagawa et al., 2005].

In the future, we are planning to strengthen this study utilizing other satellites, especially Geosynchronous Satellites, data to see how the equatorial electrojet and equatorial ionization anomaly phenomena are correlated. In addition, we want to compare the results obtained from this study with that of ground based radar electric field measurements.

Acknowledgements

I would like to give the priority of my great thank to the "Almighty God" for the uncountable gifts I have received from Him throughout my life.

The next big contributor for seeing this out come is my advisor Dr. Esayas Belay. I would like to thank him for his invaluable support, encouragement, supervision and useful suggestions throughout this research work. His moral support and continuous guidance enabled me to complete my work successfully.

I am grateful to my parents for their patience and *love*. Without them this work would never have come into existence (literally).

This study would not have been in its final form without the moral and technical supports of all my friends. Especially, I do not forget the contributions of Biaizenilign Solomon (Biz), Sefani Berhanu and his family, Ewunetu Bantie, Asiratemedhin Bekele. I should also mention Desalegn Bizuneh and Temesgen Gebremariam for their support in sending my salary on time while I was in Addis Ababa for my graduate study.

Finally, I wish to thank the Amhara National Regional State Education Bureau for the sponsorship provided to complete my graduate study.

Tamirat Bekele, Addis Ababa
August, 2008

Bibliography

[1] Abdu, M. (2001), Outstanding problems in the equatorial ionosphere-thermosphere electrodynamics relevant to spread F, J. Atoms. Sol. Terr. Phys., 63, 869-884.

[2] Abur-Robb M. F. K. and Windle D. F., 1969, Planet. Space Sci. 17, 97.

[3] Appleton, E. V., "Two Anomalies in the ionosphere", Nature, Vol. 157, p 91, 146.

[4] Baxter R. G. and Kendall P. C., 1968, Proc. R. Soc. **A304**, 171.

[5] Eccles, J. V., 1998a. Modeling investigation of the evening pprereversal enhancement of the zonal electric field in the equatorial ionosphere. Journal of Geophysical Research 103, 26709.

[6] Farley, D. T., Bonelli, E., Fejer, B. G., Larsen, M. F., 1986. The prereversal enhancement of the zonal electric field in the equatorial ionosphere. Journal of Geophysical Research 91, 13723.

[7] Fejer, B. G., E. R. de Paula, R. A. Heelis, and W. B. Hanson(1995), Global equatorial Ionospheric vertical plasma drifts measured by the AE-E satellite, J. Geophys. Res.,100, 5769-5776.

[8] Hearendel, G., Eccles, J. V., 1992. The role of the equatorial electrojet in the evening ionosphere. Journal of Geophysical Research 97, 1181.

[9] Heelis R. A., Journal of Atmospheric and Solar Terrestrial Physics 66 (2004).

[10] Heelis, R. A., Kendall, P. C., Moffett, R. J., Windle, D. W., Rishbeth, H., 1974. Electrical coupling of the E- and F-regions and its effect on F-region drifts and winds. Planetary and Space Science 22, 743.

[11] Kelley M. C, The Earth's Ionosphere: Plasma Physics and Electrodynamics, ACADEMIC PRESS, 2003.

[12] Richmond A. D., Handbook of Atmospheric Electrodynamics, Vol II, 249-290, 1995.

[13] Rishbeth, H., 1971b. Polarization fields produced by winds in the equatorial F region. Planetary and Space Science 19, 357.

[14] Rishbeth, H. (2000), The equatorial F layer layers: Progress and puzzles, Ann. Geophys., 18, 730-739.

[15] Rush C. M., and A. D. Richmond, The relationship between the structure of the equatorial anomaly and the strength of the equatorial eletrojet, Journal of Atmospheric and Terrestrial Physics, 1973, Vol. 35, pp. 1171-1180.

[16] Sagawa, E., T. J. Immel, H. U. Frey, and S. B. Mende (2005), Longitudinal structure of the equatorial anomaly in the nighttime ionosphere observed by IMAGE/FUV, J. Geophys. Res., 110, A11302, doi:10, 1029, 2004JA010848.

[17] Sterling D. L., Hanson W. B.,Moffett R. G. and Baxter R. G.,1969, Radio Sci. **4**, 1005.

Declaration

I hereby declare that this thesis is my original work and has not been presented for a degree in any other university. All sources of material used for the thesis have been duky acknowledged.

Name: Tamirat Bekele
signature: .....

This thesis has been submitted for the examination with the approval as university advisor.

Name: Dr. Esayas Belay
signature: .....

Addis Ababa University
Department of Physics
August, 2008